ACS Catalysis

pubs.acs.org/acscatalysis Research Article

Switching the Symmetry of a Trinuclear Copper Cluster Catalyst for Electroreducing CO_2 to an Asymmetric C_2 Product in an Acidic Electrolyte

Rui Wang,[§] Long-Zhang Dong,[§] Jing-Wen Shi, Mi Zhang, Shun-Li Li, Ya-Qian Lan,* and Jiang Liu*

Cite This: *ACS Catal.* 2024, 14, 741−750 Read Online

ACCESS | Metrics & More | Article Recommendations | Supporting Information

ABSTRACT: Achieving CO_2 electroreduction in an acidic electrolyte to obtain high-value products is a great challenge, but it has remained elusive so far due to the high requirements for catalyst stability. Herein, we designed and constructed a highly stable (acid- and alkali-resistant) and well-defined crystalline coordination compound catalyst, **Inz-Cu$_3$**, which can switch the structural symmetry by varying the distance and angle between the adjacent synergistic Cu active sites, thus achieving the selective conversion of CO_2 to a high-value C_2 product in an acidic electrolyte. At a current density of −320 mA·cm^{-2}, it achieved up to 42.20% selectivity for the electrocatalytic reduction of CO_2 to C_2 products in an acidic electrolyte, and the highly selective catalytic conversion to C_2 products (66.79%, containing 35.27% $FE_{C_2H_4}$ and 31.52% $FE_{C_2H_5OH}$) can also be achieved in a conventional alkaline electrolyte. Moreover, the density functional theory (DFT) calculation and control experiments revealed that the adjacent asymmetric Cu active sites with close distance can stabilize *CHOHCH$_3$ intermediates, thus improving the selectivity of the asymmetric C_2 product. This work demonstrates a strategy for the structural design of asymmetric crystalline coordination catalysts and enables the achievement of electroreduction conversion of CO_2 to high-value-added C_2 products in an acidic electrolyte.

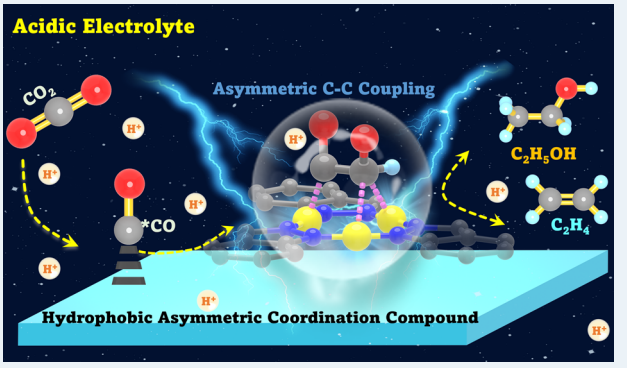

KEYWORDS: *coordination compound, symmetry, electrocatalytic CO_2 reduction, acidic electrolyte, asymmetric C−C coupling*

INTRODUCTION

Most of the current CO_2 reduction reaction (CO_2RR) systems are developed under alkaline or neutral conditions, accumulating a large amount of data and experience.[1,2] The use of alkaline electrolytes such as potassium hydroxide can improve the conductivity of the electrolytes and effectively suppress side reactions such as hydrogen generation, improving the selectivity of CO_2 conversion. In addition, some valuable carbon-based products such as methane (CH_4) and some multicarbon products are mainly generated under alkaline conditions. However, the main disadvantages of the electrochemical reduction of CO_2 under alkaline conditions are as follows: (i) Carbonate ions generated under alkaline conditions tend to accumulate on the surface of electrocatalysts, hindering the removal of products and reducing activity.[3] (ii) Some small-molecule organic acid products such as formic acid and acetic acid will continue to react under alkaline conditions, leading to side reactions and reduced selectivity. (iii) The corrosive effects under alkaline conditions may reduce the service life of the electrocatalytic system.[4] In contrast, the advantages of CO_2 reduction systems under acidic conditions are very significant.[5] First, the higher solubility of CO_2 under acidic conditions allows the catalysts to directly reduce CO_2 to products without first converting to carbonate intermediates, effectively reducing the risk of carbonate precipitation and poisoning of active sites. Furthermore, some small-molecule organic acids produced under acidic conditions, such as formic acid (HCOOH) and acetic acid (CH_3COOH), are more easily recovered from the solution. Therefore, developing CO_2 reduction electrocatalytic systems under acidic conditions can avoid or mitigate these disadvantages and help improve reaction efficiency and product value.[6]

In the past few years, the electroreduction of CO_2 to C_1 products has been widely studied,[7,8] and the selectivity of the reduction products (e.g., carbon monoxide (CO),[9−11] formic acid/formate ($HCOOH/HCOO^-$),[12−14] and methane[15]) has

Received: August 11, 2023
Revised: December 3, 2023
Accepted: December 20, 2023

Downloaded via SOUTH CHINA NORMAL UNIV on January 12, 2024 at 12:32:38 (UTC).
See https://pubs.acs.org/sharingguidelines for options on how to legitimately share published articles.

© XXXX American Chemical Society

https://doi.org/10.1021/acscatal.3c03755
ACS Catal. 2024, 14, 741−750

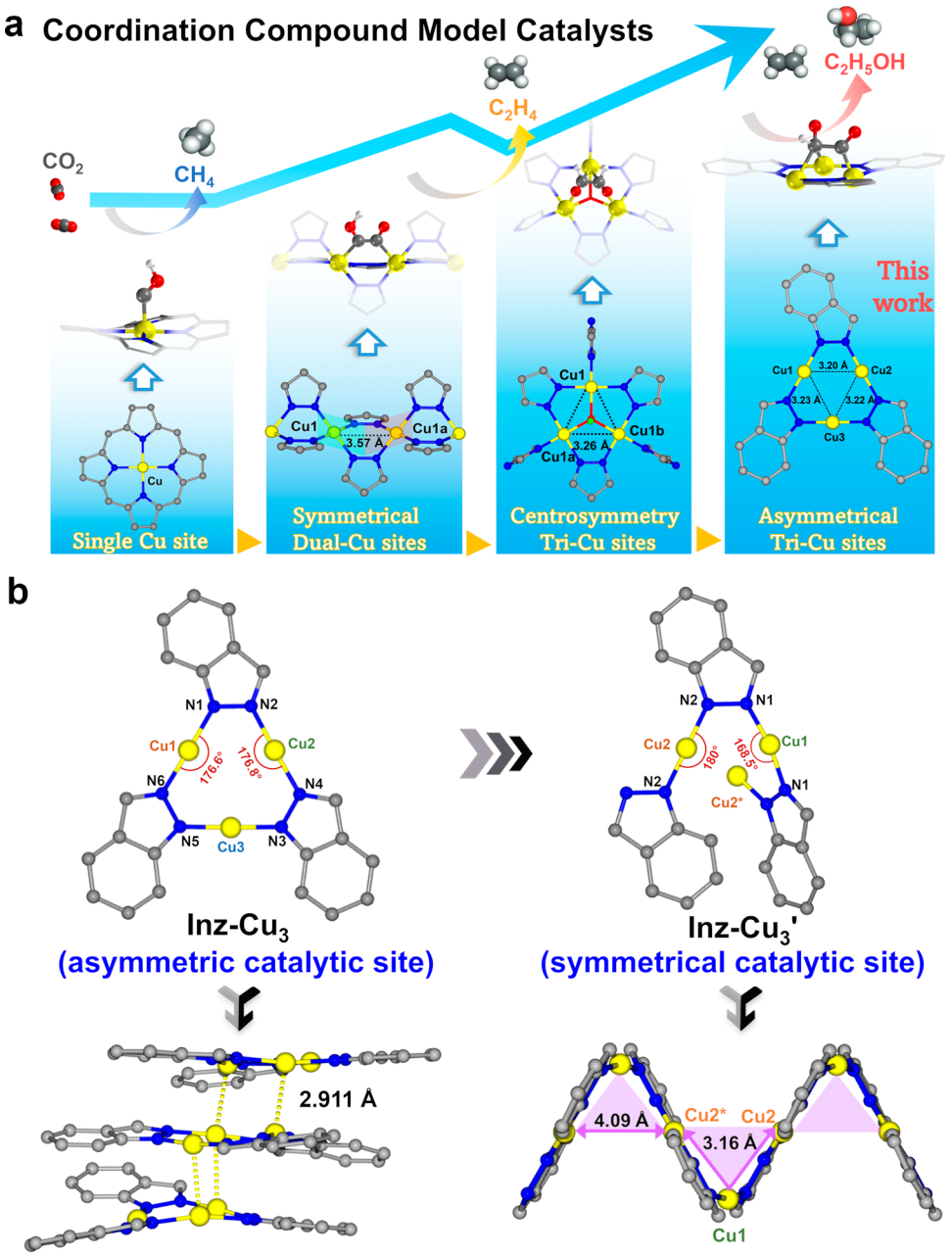

Figure 1. (a) Crystalline coordination catalyst design evolution gradually upgrades the CO_2 reduction products. (b) Structural transformation from **Inz-Cu$_3$** to **Inz-Cu$_3$′**. Color code: C, black; N, blue; Cu, yellow. All hydrogen atoms have been omitted for clarity.

reached or exceeded 80%. Thus, the current research hotspots have shifted to the generation of C_2 products with higher energy density.[16,17] Copper-based catalysts are currently considered to be the most important type of catalysts for the conversion of CO_2 to high-value carbon-based products.[18−20] So far, it has been inferred from many copper-based catalyst systems that symmetrical catalytic active sites are more inclined to produce symmetrical C_2 products under alkaline conditions, with particular attention to coordination compound catalysts.[21,22] Coordination compounds with precise structural information have significant advantages in the study of the mechanism of the electrocatalytic CO_2 reduction reaction (CO_2RR). In our previous work, by adjusting the number, distance, and angle of catalytic active sites in copper-based coordination compound catalysts, we gradually realized the conversion of CO_2 reduction products from C_1 to symmetrical C_2 products (Figure 1a).[23−27] It can be demonstrated that establishing appropriate copper-based coordination compound catalyst models may effectively regulate the selectivity of carbon-based reduction products as well as help in better understanding the mechanism of the catalytic reaction. In order to improve the overall efficiency of the C_2 product, we also need to consider the conditions for the generation of liquid-phase asymmetric C_2 products (e.g., ethanol (C_2H_5OH)). However, little is known about the conditions that need to be met by a catalyst to produce an asymmetric C_2 product, and it is important and necessary to find a suitable catalyst system to further explain the catalytic mechanism for the reduction of CO_2 to an asymmetric carbon-based product.[28] Based on the above design considerations, it is hoped that the conversion of CO_2 to an asymmetric C_2 product by coordination compound model catalysts will

https://doi.org/10.1021/acscatal.3c03755
ACS Catal. 2024, 14, 741−750

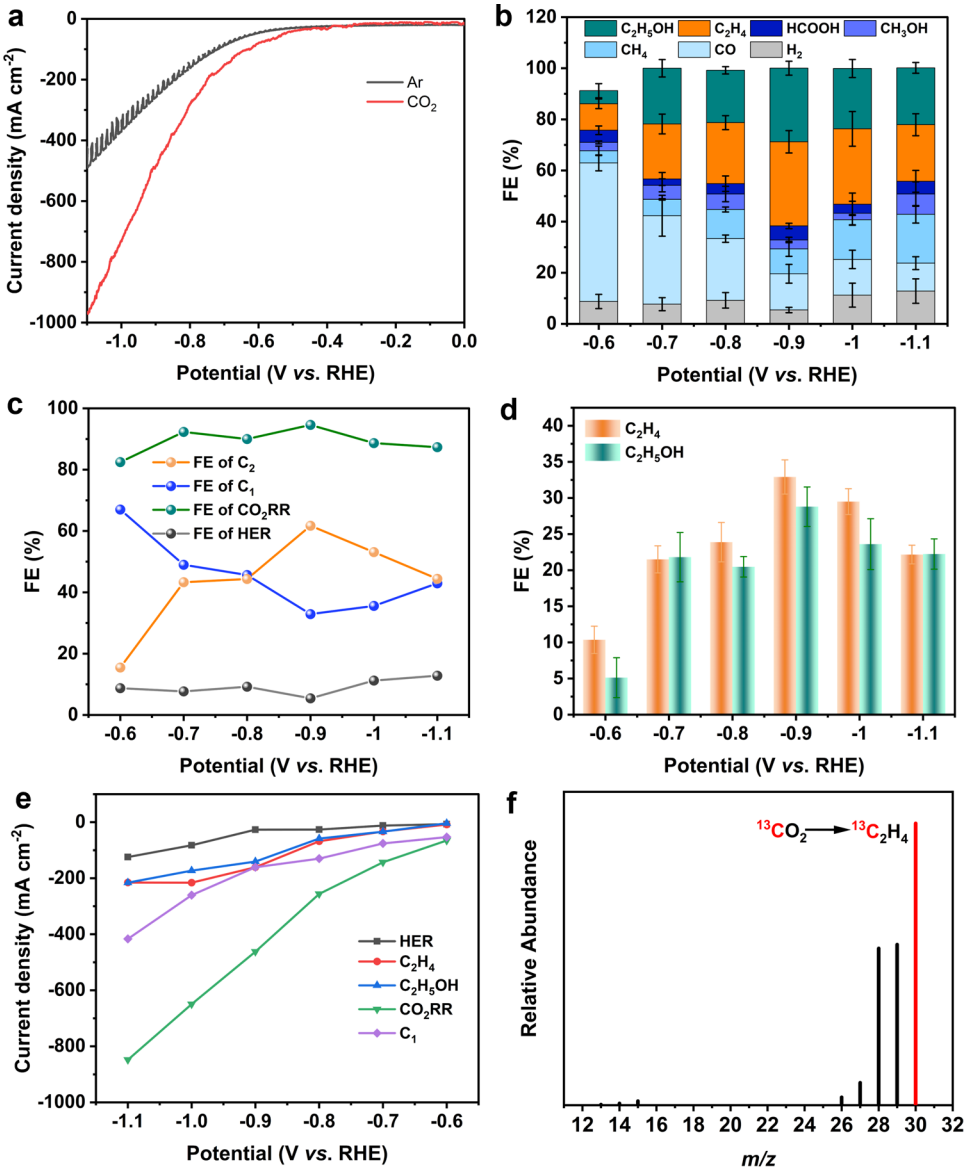

Figure 2. Electrocatalytic performances of **Inz-Cu$_3$** in 1 M KOH. (a) LSV curves. (b) Faradaic efficiency (FE) of different reduction products. (c) The contrast of FE (H_2, CO_2RR, C_1, and C_2) at −0.6 to −1.0 V versus RHE. (d) The contrast FE of C_2H_4 and C_2H_5OH. (e) The partial current density of different reduction products. (f) The mass spectra from GC-MS of the $^{13}C_2H_4$ product from $^{13}CO_2$ reduction.

continue. Given that the asymmetric products still need to complete the C−C coupling reaction during the reduction process, we speculate that the catalyst model for the efficient electroreduction of CO_2 to an asymmetric C_2 product should contain at least two adjacent active sites with close distance and different coordination environments, which may lead to the completion of the asymmetric C−C coupling of key reaction intermediates in the CO_2RR process and thus facilitate the conversion of CO_2 to asymmetric carbon-based products.[29]

In order to improve the selectivity of electrocatalytic CO_2 to generate C_2 products, this work continued to improve the cyclic symmetrical Cu_3N_6 structure and constructed an ultrastable and well-defined trinuclear copper-based cluster compound by combining an indazole ligand with copper salts, {Cu_3 (μ-Inz)$_3$} (denoted **Inz-Cu$_3$**, **Inz** = 1*H*-Indazole), exhibiting high hydrophobicity and chemical stability in a strong acid−base environment. When **Inz-Cu$_3$** was applied as an electrocatalyst for CO_2RR, it exhibited the highest selectivity for CO_2 electroreduction to C_2 of 66.79% (containing 35.27% $FE_{C_2H_4}$ and 31.52% $FE_{C_2H_5OH}$) at −0.9 V (vs reversible hydrogen electrode, RHE) in an alkaline electrolyte. Meanwhile, **Inz-Cu$_3$** still showed a good selectivity of 42.20% for C_2 products at a current density of −320 mA·cm^{-2} in an acidic electrolyte (pH = 2), which implies that the coordination compound catalyst can realize the conversion of CO_2 to the C_2 product in an acidic environment. As predicted, comparative experiments and theoretical calculations demonstrate that the asymmetric Cu active site in **Inz-Cu$_3$** achieves asymmetric C−C coupling by adsorbing two forms of *CO and then stabilizing the *$CHOHCH_3$ intermediate, allowing for the selective reduction of CO_2 to asymmetric C_2 products. This work reveals how the conversion of CO_2 to symmetric or asymmetric C_2 products can be achieved by modulating the symmetry of the active site.

https://doi.org/10.1021/acscatal.3c03755
ACS Catal. 2024, 14, 741−750

RESULTS AND DISCUSSION

Synthesis of Inz-Cu$_3$. $Cu(NO_3)_2{\cdot}3H_2O$ (0.3 mmol), indazole (Inz, 0.3 mmol), DMF (5 mL), and 0.1 M KOH solution (2 mL) were mixed and heated at 100 °C for 24 h; after cooling at room temperature, a large number of colorless long flake crystals were obtained, named **Inz-Cu$_3$**. Single-crystal X-ray diffraction analysis (SCXRD) reveals that **Inz-Cu$_3$** crystallizes in the orthorhombic space group *P*bca (Table S1). During the structure resolution, there is dynamic disorder in the ligand at the positions of the bridging Cu1 and Cu2 atoms, and one set of structures was selected for analysis to understand the structural details more clearly (Figure S1). As shown in Figure 1b, any two Cu atoms in this structure are bridged by three Inz ligands and finally form a twisted cycle triangular trinuclear Cu-based cluster compound, $\{Cu_3(\mu\text{-}Inz)_3\}$. The overall structure of **Inz-Cu$_3$** is noncoplanar and does not have symmetry (Figure S2). It contains three Cu atoms with different coordination environments, which are not bonded to any ligand in the axial position and without any solvent molecules at the center position; such a coordination pattern provides enough spatial environment for the adsorption of small gas molecules. The values of bond lengths and bond angles selected in the crystal structure are listed in Table S2. In addition, due to the weak cuprophilic interaction (the Cu···Cu distance = 2.91 Å) between the Cu1 atom and the Cu3 atom of another adjacent trinuclear cluster, **Inz-Cu$_3$** finally exists as a dimer in the crystal structure (Figure S3).

Characterization of Inz-Cu$_3$. To evaluate the crystallinity and chemical stability of **Inz-Cu$_3$**, powder X-ray diffraction (PXRD) experiments were carried out on the as-synthesized sample. Figure S4 shows that the PXRD patterns of the synthesized samples are in good agreement with the simulated pattern of single-crystal data, indicating high purity and crystallinity. Next, 30 mg of the synthesized crystals were submerged for 24 h in 10 mL of 1 M KOH solution (pH 14) and 10 mL of 0.5 M K_2SO_4 solution (pH 2, adjusted with sulfuric acid), respectively. **Inz-Cu$_3$** can still preserve its structural integrity in a highly acidic and alkaline solution, as shown by the PXRD patterns of the soaked crystals being consistent with the intrinsic PXRD patterns of the crystalline samples. The structural characteristics and stability of **Inz-Cu$_3$** were further revealed by Fourier transform infrared spectroscopy (FTIR) experiments (Figure S5). Furthermore, thermogravimetric analysis (TGA) was performed in an oxygen environment to evaluate the sample's thermal stability. The curve demonstrates that **Inz-Cu$_3$** could retain structural stability up to 280 °C (Figure S6). Most important of all, the apparent contact angle of **Inz-Cu$_3$** was tested with deionized water at room temperature. The test result shows that **Inz-Cu$_3$** has a contact angle close to 122°, thus proving that **Inz-Cu$_3$** has higher hydrophobicity (Figure S7). Overall, the high structural and chemical stability of **Inz-Cu$_3$** serves as a crucial foundation for investigating the development of its performance.

Electrochemical CO_2 Reduction Performance. Given the chemical stability of **Inz-Cu$_3$**, it can be used as an electrocatalyst to evaluate the electrocatalytic CO_2RR performance in flow cell.[19] The gas diffusion layer (GDL) uniformly coated with electrocatalyst suspension was used as a working electrode. Platinum tablets and a saturated Ag/AgCl electrode were used as the counter and reference electrodes, respectively. The linear sweep voltammetry (LSV) curves were measured in CO_2 and Ar streams separately. Figure 2a demonstrates that the onset potential of **Inz-Cu$_3$** in a CO_2 atmosphere is more positive than that in an Ar atmosphere, and the current density in the CO_2 stream is much higher than that in the Ar stream, confirming its higher reaction activity of electrocatalytic CO_2RR than the competitive hydrogen evolution reaction (HER).[30] To explore the electrocatalytic selectivity for different reduction products of **Inz-Cu$_3$**, the CO_2 electroreduction experiments were carried out at the selected potential range (−0.6 to −1.1 V) in an alkaline electrolyte. The gas product obtained is analyzed by online gas chromatography (7820A, Agilent), which was equipped with a flame ionization detector (FID) and a thermal conductivity detector (TCD). The liquid-phase products are qualitative and quantitative by ^{1}H NMR, ion chromatography (IC), and headspace gas chromatographic analysis (HS-GC). The corresponding product distribution and specific error bars at different potentials are displayed in Figure 2b and Table S3. As the applied cathodic potential increases, the FE of CO decreases gradually and the C_2 product (referred to as C_2H_4 and C_2H_5OH) shows an obvious competitive advantage. To be specific, the **Inz-Cu$_3$** catalyst gives 54.22% FE_{CO}, 10.35% $FE_{C_2H_4}$, 5.12% $FE_{C_2H_5OH}$, and 8.74% FE_{H_2} at −0.6 V. In addition, there are other products, such as CH_4, HCOOH, and methanol (CH_3OH), whose selectivity is less than 10%. When the potential comes to −0.9 V, FE_{C_2} increases in a volcanic plot trend and achieves its peak value of 66.79% (including 35.27% $FE_{C_2H_4}$ and 31.52% $FE_{C_2H_5OH}$; Figure 2c,d). It is worth noting that FE_{C_2} remains higher than 44.34% from −0.8 to −1.1 V. FE_{H_2} is always lower than 15% at all applied potentials, which signifies the poor selectivity for HER of **Inz-Cu$_3$**. FE_{CO_2RR} remains at a high level (over 82.46%) in the potential range from −0.6 to −1.1 V, demonstrating that **Inz-Cu$_3$** provides superior selectivity for CO_2 conversion to high-value-added products. ^{1}H NMR also qualitatively detects CH_3OH, C_2H_5OH, and other cathodic liquid-phase products (Figure S8). To further reveal the electrocatalytic activity of **Inz-Cu$_3$**, the partial current densities of H_2, C_2H_4, C_2H_5OH, CO_2RR, and C_1 have been calculated (Figure 2e). Meanwhile, to verify the carbon source of the reduction product, the ^{13}C isotope labeling experiment was carried out by using $^{13}CO_2$ instead of $^{12}CO_2$ under the same reaction conditions. The results of gas chromatography−mass spectrometry show that the peaks at m/z = 29, 17, and 30 are, respectively, assigned to ^{13}CO, $^{13}CH_4$, and $^{13}C_2H_4$, indicating that the carbon-based reduction products indeed derive from the CO_2 used (Figures 2f and S9).

To reveal that the symmetry of catalytically active sites affects the catalytic selectivity of catalysts in the CO_2RR process, the Cu−dimethylpyrazole complex (**DMPz-Cu$_3$**) was synthesized as a contrastive sample.[31,32] Similarly, the **DMPz-Cu$_3$** structure has a cyclic trinuclear Cu active site and exists as dimers as a result of a weak cuprophilic interaction. In contrast to **Inz-Cu$_3$**, its overall structure is centrosymmetric (Figure S10). When it is used as an electrocatalyst under the same CO_2RR test conditions as **Inz-Cu$_3$**, **Inz-Cu$_3$** exhibits a higher current density than **DMPz-Cu$_3$** at each potential, which further implies the better electrocatalytic activity of **Inz-Cu$_3$** (Figure S11). As the applied cathodic potential gradually increases, FE_{CO} gradually decreases, while the FE of CH_4 and C_2H_4 progressively grows. At −0.9 V, the maximum FE of C_2H_4 can reach 29.10%. Once the performance of the two

https://doi.org/10.1021/acscatal.3c03755
ACS Catal. 2024, 14, 741−750

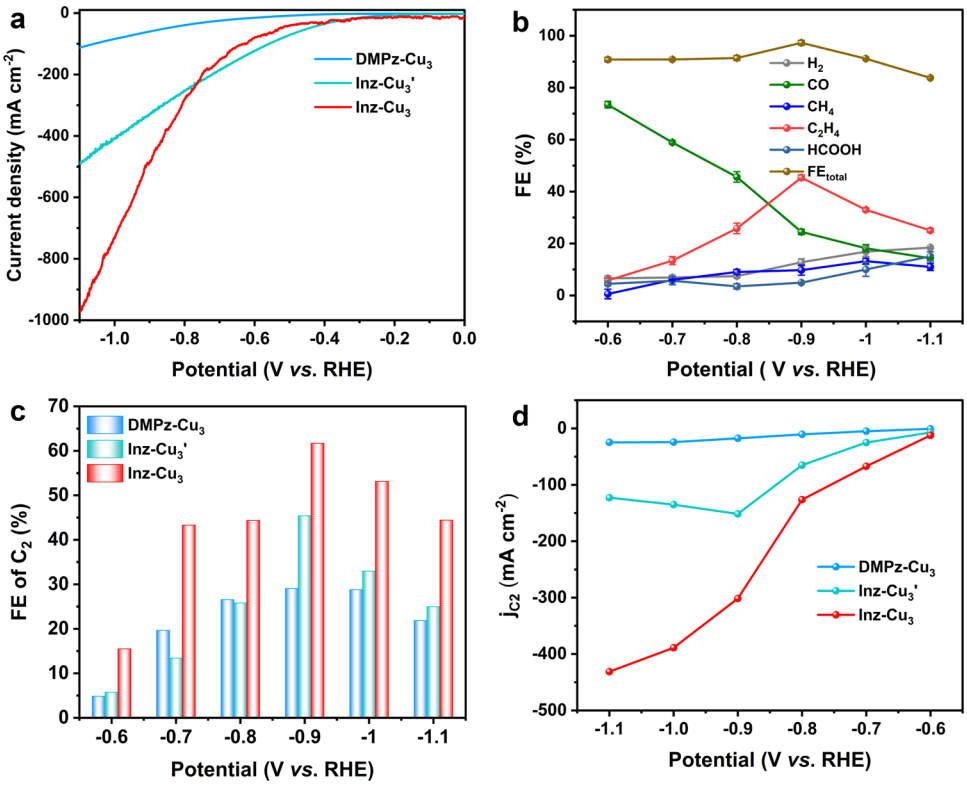

Figure 3. (a) LSV curves. (b) Electrocatalytic performances of **Inz-Cu$_3$′** in 1 M KOH. (c) The contrast FE of the C_2 products. (d) The partial current density of C_2 at different applied potentials.

catalysts is contrasted, it is obvious to discern that the main product of **DMPz-Cu$_3$** with higher cuprophilic interactions is CH_4, with C_2H_4 as the secondary product and the trace liquid-phase C_2H_5OH product being negligible. By comparing the FE of C_2 products of the two catalysts at all test potentials, it can be found that **Inz-Cu$_3$** has better selectivity for C_2 products in the CO_2RR process, and the selectivity of C_2H_5OH remains above 20% in a wide voltage range (−0.7 to −1.1 V). Through the above analysis, we speculate that the advantage of **Inz-Cu$_3$** in producing an asymmetric product (C_2H_5OH) can be attributed to the asymmetry of catalytic Cu active sites, while **DMPz-Cu$_3$** with a symmetrical Cu site prefers to produce C_2H_4.

Moreover, **Inz-Cu$_3$′** was synthesized by increasing the reaction temperature under the same conditions as **Inz-Cu$_3$**. Based on the original closed **Inz-Cu$_3$** structure, the Cu3−N5 bond is broken, and the two Inz coordinated with Cu3 flipped a certain angle, finally obtaining the M-type chain structure of the nonplanar co-top Cu3 conformation (Figures S12 and S13). Compared with the cyclic trinuclear Cu-based cluster, the structure of **Inz-Cu$_3$′** with a similar Cu3 conformation and symmetric catalytic active site undergoes a spatial conformational change. Besides, **Inz-Cu$_3$′** also possesses high chemical stability and hydrophobicity (Figures S14−S16). To verify whether the above conclusions are reasonable, the electroreduction of the CO_2 reaction experiments was carried out in the selected potential range (−0.6 to −1.1 V) using **Inz-Cu$_3$′** as an electrocatalyst. From Figure S17, the LSV curve shows that the current density of **Inz-Cu$_3$** is twice that of **Inz-Cu$_3$′**. In addition, H_2, CO, CH_4, and C_2H_4 were analyzed as the main gaseous products, and the FE_{total} of the gaseous products was almost 100%, and almost no liquid product was found by ^{1}H NMR (Figures 3 and S18). As the cathodic potential increases, the FE of C_2H_4 impressively increases to a maximum of ∼50.0% at −0.8 V. By comparing the FE_{C_2} values of the two catalysts at the same potential, it is possible to conclude that catalytic selectivity is altered as the catalytic active site transitions from a symmetric to an asymmetric state. The symmetric active site prefers a symmetric C−C coupling to make C_2H_4, but the asymmetric catalytic active site decreases the chemical difficulty in generating C_2H_5OH in competition with C_2H_4 formation.[33] This hypothesis is supported by the experimental results, which validate the viability of **Inz-Cu$_3$** as a catalyst in the production of asymmetric carbon-based products.

To further explore the potential factors for the difference in the electrocatalytic performance of the two catalysts, we explored the reasons from the perspective of reaction kinetics. First, the electrochemical double-layer capacitance (C_{dl}) values have been calculated from the cyclic voltammogram (CV) curves to estimate the electrochemical active surface area (ECSA). As shown in Figure S19, the C_{dl} values of **Inz-Cu$_3$** and **Inz-Cu$_3$′** are 0.85 and 13.41 mF·cm^{-2}, respectively, demonstrating that **Inz-Cu$_3$′** with symmetrical active site possesses more available active sites interacting with the electrolyte.[26] To explore the catalytic durability properties of these catalysts for further applications, the long-term durability of **Inz-Cu$_3$** was assessed by the chronoamperometric curve at −0.9 V, the potential that has achieved the optimal selectivity for the CO_2-to-C_2 conversion. The result illustrates that **Inz-Cu$_3$** can maintain the current density of approximately −400 mA·cm^{-2} and FE_{C_2} over 60.00% during the continuous electrolysis of 8000 s (Figure S20). In comparison, the **DMPz-Cu$_3$** catalyst displays poor catalytic stability during the long-term test. The catalytic stability of another comparative

https://doi.org/10.1021/acscatal.3c03755
ACS Catal. 2024, 14, 741−750

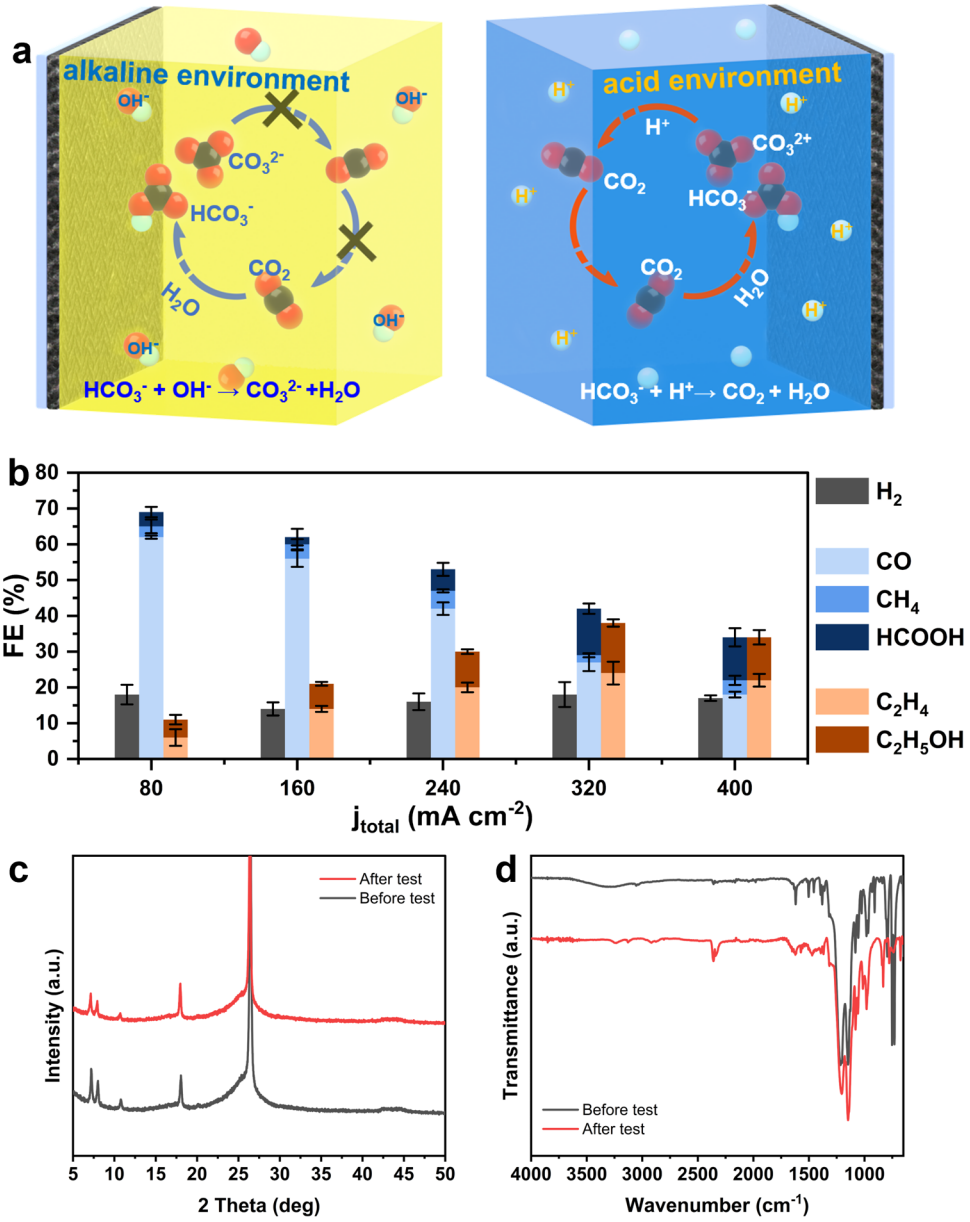

Figure 4. (a) Carbon mass transfer diagram in alkaline and acidic environments. (b) Electrocatalytic performances of **Inz-Cu$_3$** in an acidic electrolyte. (c, d) The PXRD and FTIR patterns of **Inz-Cu$_3$**-modified GDL-carbon paper electrodes before and after tests.

sample, **Inz-Cu$_3$′**, in a prolonged test is shown in Figure S21, where the **Inz-Cu$_3$′** catalyst can maintain a current density of ∼−330 mA·cm^{-2} and more than 45.00% $FE_{C_2H_4}$ during continuous electrolysis for 2300 s. This verifies that the stronger hydrophobicity of Inz-Cu$_3$ reduces the affinity of the electrode for water, which helps to promote the diffusion of small gas molecules and thus improves its stability in the catalytic process.[34,35] However, the durability of the electrocatalysis is somewhat limited due to the harsh electrolysis conditions and the traditional carbon paper support.

In addition, in order to explore the structural stability of the **Inz-Cu$_3$** catalyst, a series of comparative characterization techniques of the working electrode were performed before and after the test. First, the morphology of the **Inz-Cu$_3$** catalyst remains basically unchanged before and after electrolysis from the SEM images of the uniformly ground samples (Figure S22). The PXRD, FTIR, and XPS patterns of **Inz-Cu$_3$** before and after the test are well-matched, indicating that they could retain structural integrity in the CO_2RR process (Figures S23−S25). The XAS measurement results show that no significant change in Cu K-edges could be observed in the X-ray absorption near edge structure (XANES) profiles of **Inz-Cu$_3$** after the electrocatalytic process (Figure S26), and no obvious change in the Cu−Cu distance is observed in the extended X-ray absorption fine structure (EXAFS) spectrum. At the same time, the test results also verified that the oxidant state of Cu(I) in **Inz-Cu$_3$** was found to be unchanged, which indicated that the Cu(I) centers were not reduced to Cu(0) particles or turned into Cu_2O or CuO.[36] All of the aforementioned results demonstrate that **Inz-Cu$_3$** as a persistent heterogeneous catalyst has superior activity for the electrochemical conversion of CO_2 to C_2. For **Inz-Cu$_3$′**, it can be found that the catalyst largely maintains its original morphology by comparing the SEM images before and after the test (Figure S27). Moreover, the PXRD patterns of **Inz-Cu$_3$′** before and after the test proved

https://doi.org/10.1021/acscatal.3c03755
ACS Catal. 2024, 14, 741−750

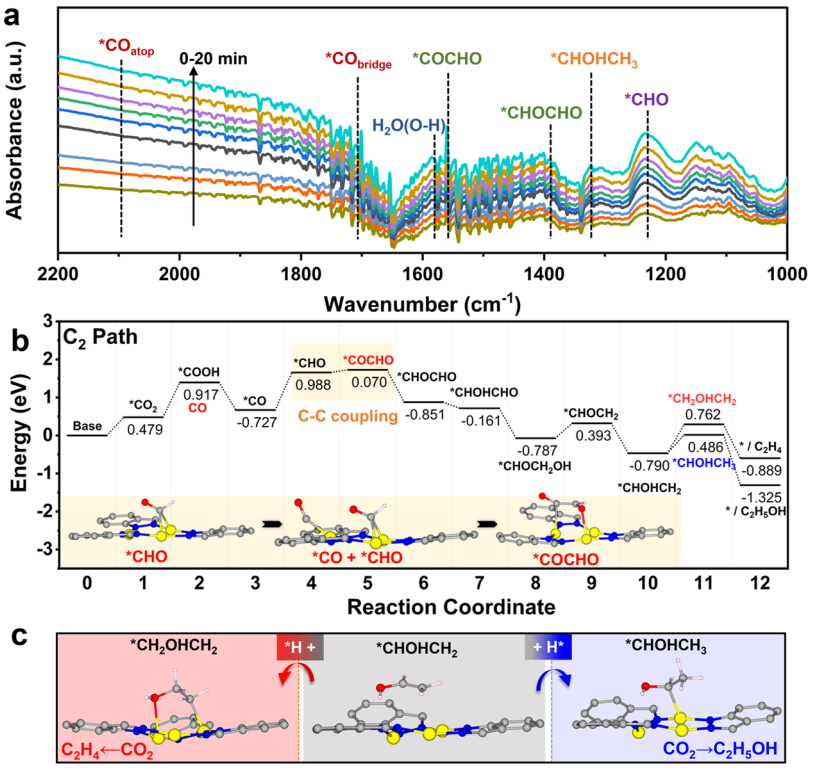

Figure 5. In situ DRIFTS and DFT calculations. (a) Time-dependent in situ DRIFTS spectra for CO_2RR on **Inz-Cu$_3$**. (b) Gibbs free energy profiles for the dimerization of *CO to C_2H_4 and C_2H_5OH. (c) The important intermediate for generating C_2H_4 and C_2H_5OH.

that the sample did not have any phase change during the catalytic process (Figure S28). The FTIR spectra of **Inz-Cu$_3$′** before and after the test also confirmed the above conclusion (Figure S29). Though the spatial configuration of **Inz-Cu$_3$** has been transformed, **Inz-Cu$_3$′** still has high stability and catalytic activity.

Although alkaline or neutral pH electrolytes are typically used to minimize competitive HER, they can also result in carbonate formation, which is harmful to boosting CO_2 utilization efficiency.[37,38] In contrast, an acidic medium can aid in overcoming the carbon utilization limit in neutral and alkaline solutions by minimizing the formation of carbonates (Figure 4a).[6,39,40] Moreover, the higher proton concentration in the electrolyte and the use of a Nafion membrane as a separator are expected to minimize carbonate formation and liquid product crossover. Considering the stability of **Inz-Cu$_3$** in acidic solutions, it could be used as an electrocatalyst to evaluate the CO_2RR performance in a flow cell using 0.5 M K_2SO_4 (pH adjusted to 2.0 with sulfuric acid) aqueous solution as an electrolyte.[6] Figure 4b and Table S4 show the product distribution of CO_2RR on **Inz-Cu$_3$** in the current density range (-80 to -400 mA·cm^{-2}). FE_{H_2} is essentially identical to that of an alkaline environment, which is less than 20%. This result proves that the catalyst can effectively inhibit HER under any test environment. As the applied current increases, the selectivity of the C_1 product decreases gradually, while the FE of the C_2 product increases steadily. At -320 mA·cm^{-2}, the **Inz-Cu$_3$** catalyst gives the highest FE for C_2 products of 42.20%, with a partial current density of -135.04 mA·cm^{-2}. So far, there has been no report on the application of crystalline materials in electrocatalytic CO_2RR in acidic solution (Table S5). The long-term durability of **Inz-Cu$_3$** is tested under the condition of -320 mA·cm^{-2}. The chronoamperometric curve (Figure S30) shows that $FE_{C_2H_4}$ remains at about 20% during the durability test of 9 h. It can be seen that the acidic electrocatalytic system can greatly improve the catalytic stability of the catalyst. Furthermore, the PXRD and IR patterns of **Inz-Cu$_3$** before and after the test are well-matched, showing no significant structural changes (Figure 4c,d).

In Situ DRIFTS Characterization. To further monitor reaction intermediates associated with multicarbon C_2H_5OH production on **Inz-Cu$_3$** in the CO_2RR process, the time-dependent in situ diffuse reflectance infrared Fourier transform spectroscopy (DRIFTS) is employed to infer the reaction pathway. As shown in Figure 5a, the DRIFTS spectra for this catalyst exhibit several possible reaction intermediates with the cathode potential at -0.9 V. In specific, the two peaks at ∼2096 and ∼1704 cm^{-1} are associated with the atop-adsorbed *CO (*CO_{atop}) and bridge-adsorbed *CO (*CO_{bridge}) on **Inz-Cu$_3$**, respectively, which verifies that the presence of two adsorption forms of *CO in **Inz-Cu$_3$** provides the possibility for the occurrence of asymmetric C−C coupling to C_2H_5OH.[41,42] The peaks located at ∼1235 cm^{-1} growing conspicuously with increasing test time can be designated to *CO protonation (*CHO).[43] Additional peaks at ∼1576 and ∼1397 cm^{-1} are indexed to the absorbed *OCCHO and *CHOCHO, respectively, strong evidence for the direct CO−CO dimerization on **Inz-Cu$_3$**.[44,45] More importantly, the growing peak at ∼1318 cm^{-1} is ascribed to the C−H bending vibration of *$CHOHCH_3$, which is considered as the key intermediate for C_2H_5OH production.[46] This may be attributed to the asymmetric C−C coupling-induced unbalanced coordination environment, which disrupts the coordination sites of the C_2H_4 intermediate and stabilizes the C_2H_5OH intermediate. This conclusion is consistent with reports that the diversity of *CO binding sites enhances the

https://doi.org/10.1021/acscatal.3c03755
ACS Catal. 2024, 14, 741−750

formation of C_{2+} liquid products.[44] Therefore, this work hypothesizes that activated asymmetric C−C coupling on **Inz-Cu$_3$** favors the C_2H_5OH pathway via stabilizing crucial intermediates.

DFT Calculations. Based on the well-defined catalytic model (Figure S31), DFT calculations are performed to investigate the reaction mechanism of the CO_2RR to C_2 products. The Gibbs free energy energies of the possible intermediates from different pathways of CO_2 reduction to C_2H_4 and C_2H_5OH have been calculated (Figure S32 and Table S6). The CO_2 gas molecules are first adsorbed on the catalytic Cu sites and then undergo protonation (*COOH) and dehydration for *CO. The above reduction process indicates that the close Cu···Cu distance and a large amount of catalytic Cu sites in **Inz-Cu$_3$** are more likely to stabilize the *CO intermediate and then hydrogenate to obtain *CO-(H)$_{bridge}$. Subsequently, *CO(H)$_{bridge}$ is coupled with *CO$_{atop}$ to generate the *COCHO intermediate, which is adsorbed on two Cu sites with one C-terminal binding and another O-terminal binding, and the resulting asymmetric C−C coupling reaction contributes to increased C_2 production. After multistep proton-coupled electron transfer (PCET) steps, the *COCHO intermediate is successively reduced to *CHO-CHO, *CHOHCHO, *CHOCH$_2$OH, *CHOCH$_2$, and *CHOHCH$_2$.[47] The relevant structures of the reaction intermediates involved in the proposed reaction mechanism for the CO_2RR to C_2 on the **Inz-Cu$_3$** catalyst are shown in Figure S33. Notably, the reaction pathways to produce C_2H_4 and C_2H_5OH are identical on **Inz-Cu$_3$**, as their initial adsorption of CO_2 starts and follows a series of PCET processes to finally generate a shared intermediate, *CHOHCH$_2$. Therefore, the selectivity between C_2H_4 and C_2H_5OH is significantly dependent on the adsorption capacity of the active Cu sites for the next key intermediate in both pathways. It can be seen from Figure 5b that the formation energy of *CHOHCH$_2$ → *CHOHCH$_3$ (−1.325 eV) is lower than that of *CHOHCH$_2$ → *CH$_2$OHCH$_2$ (−0.889 eV). This result indicates that the key *CHOHCH$_3$ intermediates for C_2H_5OH production are more stable on **Inz-Cu$_3$** (Figure 5c). From the perspective of the catalyst structure, the reason for this result is that **Inz-Cu$_3$** catalysts with asymmetric catalytic active sites are more likely to be activated for asymmetric C−C coupling, which provides the possibility of C_2H_5OH formation.

Currently, there are few reports on the use of coordination compounds as electrocatalysts to specifically analyze the conditions for the generation of asymmetric C_2 products. Most of the electrocatalysts on coordination compounds almost always explore C_2 products rather than asymmetric C_2 products, i.e., C_2H_4 and C_2H_5OH coexist.[48] In comparison, the asymmetric C_2 product ethanol produced by the catalysts in our work is slightly higher. In addition, the more prominent performers for the generation of asymmetric C_2 products are copper-based nanomaterials and composites, with the main synthesis strategies including crystal facet tuning,[49] doping,[50] modulation of different components,[34] and morphology regulation,[51] which have a good selectivity (>50%). Nonetheless, problems with these materials are obvious such as complex catalyst compositions and insufficiently well-defined structural information for probing the catalytic reaction mechanism for the generation of asymmetric C_2 products. Although our performance is not as good as that of nanomaterials, the original intention of our work was to utilize coordination compound models to clearly explain the structure−property conformational relationship, thus providing directions for the design and synthesis of high-performance catalysts for generating asymmetric C_2 products.

CONCLUSIONS

In summary, we designed and synthesized a highly hydrophobic trinuclear copper-based cluster compound (**Inz-Cu$_3$**) catalyst to explore the effect of an asymmetric catalytic environment on product selectivity. **Inz-Cu$_3$** contains three adjacent and close distance asymmetric Cu active sites, in which the *CO adsorption is oriented as both atop and bridge configurations to trigger symmetric and asymmetric C−C coupling for stabilization of the key intermediates. It exhibits the highest FE_{C_2} (66.79%) containing 35.27% $FE_{C_2H_4}$ and 31.52% $FE_{C_2H_5OH}$ at −0.9 V in the alkaline electrolyte. Although its catalytic effect in an alkaline environment is not outstanding, it shows a good selectivity of 42.20% for C_2 products at a current density of −320 mA·cm^{-2} in an acidic electrolyte. By comparing the electrocatalytic performance of **DMPz-Cu$_3$**, **Inz-Cu$_3$'** with the symmetric structure and **Inz-Cu$_3$** with the asymmetrical structure, the rationality of **Inz-Cu$_3$** as a crystal coordination compound model catalyst for electrocatalytic CO_2 conversion to C_2H_5OH was demonstrated. DFT calculations reveal that the presence of asymmetric Cu active sites can stabilize *CHOHCH$_3$ to boost the selective reduction of CO_2 to C_2H_5OH. This work provides a case where CO_2 can be highly selectively reduced to C_2 products in acidic environments by utilizing coordination compound catalysts.

ASSOCIATED CONTENT

Supporting Information

The Supporting Information is available free of charge at https://pubs.acs.org/doi/10.1021/acscatal.3c03755.

Detailed information regarding experimental methods; characterization analysis; and DFT calculations (PDF)

AUTHOR INFORMATION

Corresponding Authors

Ya-Qian Lan − *Jiangsu Collaborative Innovation Centre of Biomedical Functional Materials, Jiangsu Key Laboratory of New Power Batteries, School of Chemistry and Materials Science, Nanjing Normal University, Nanjing 210023, P. R. China; School of Chemistry, South China Normal University, Guangzhou 510006, P. R. China;* orcid.org/0000-0002-2140-7980; Email: yqlan@njnu.edu.cn, yqlan@m.scnu.edu.cn

Jiang Liu − *Jiangsu Collaborative Innovation Centre of Biomedical Functional Materials, Jiangsu Key Laboratory of New Power Batteries, School of Chemistry and Materials Science, Nanjing Normal University, Nanjing 210023, P. R. China; School of Chemistry, South China Normal University, Guangzhou 510006, P. R. China;* orcid.org/0000-0002-2596-4928; Email: liuj0828@m.scnu.edu.cn; http://www.yqlangroup.com

Authors

Rui Wang − *Jiangsu Collaborative Innovation Centre of Biomedical Functional Materials, Jiangsu Key Laboratory of New Power Batteries, School of Chemistry and Materials Science, Nanjing Normal University, Nanjing 210023, P. R. China*

https://doi.org/10.1021/acscatal.3c03755
ACS Catal. 2024, 14, 741−750

Long-Zhang Dong − *School of Chemistry, South China Normal University, Guangzhou 510006, P. R. China;* orcid.org/0000-0002-9276-5101
Jing-Wen Shi − *School of Chemistry, South China Normal University, Guangzhou 510006, P. R. China*
Mi Zhang − *School of Chemistry, South China Normal University, Guangzhou 510006, P. R. China*
Shun-Li Li − *School of Chemistry, South China Normal University, Guangzhou 510006, P. R. China*

Complete contact information is available at: https://pubs.acs.org/10.1021/acscatal.3c03755

Author Contributions

§R.W. and L.-Z.D. contributed equally to this work. Y.-Q.L., J.L., and R.W. conceived and designed the idea. R.W. conducted the characterization and designed the experiments. L.-Z.D. performed the DFT calculations. L.-Z.D. and J.-W.S. collected and analyzed the crystallographic data. M.Z. and S.-L.L. discussed the results and prepared the manuscript. R.W. wrote the manuscript. All of the authors reviewed and contributed to this paper.

Notes

The authors declare no competing financial interest.

■ ACKNOWLEDGMENTS

This work was financially supported by the NSFC (Grants 22271104, 92061101, 21871141, 22225109, and 22105080), the Excellent Youth Foundation of Jiangsu Natural Science Foundation (No. BK20211593), the China Postdoctoral Science Foundation (No. 2020M682748), the Guangdong Basic and Applied Basic Research Foundation (2023A1515010928), Guangzhou Basic and Applied Basic Research Fund Project (Grant 202102020209), Postgraduate Research & Practice Innovation Program of Jiangsu Province (KYCX22_1546), Priority Academic Program Development of Jiangsu Higher Education Institutions, and the Foundation of Jiangsu Collaborative Innovation Center of Biomedical Functional Materials.

■ REFERENCES

(1) Deng, B.; Huang, M.; Zhao, X.; Mou, S.; Dong, F. Interfacial Electrolyte Effects on Electrocatalytic CO_2 Reduction. *ACS Catal.* **2022**, *12* (1), 331−362.
(2) Zhang, X.; Li, J.; Li, Y.; Jung, Y.; Kuang, Y.; Zhu, G.; Liang, Y.; Dai, H. Selective and High Current CO_2 Electro-Reduction to Multicarbon Products in Near-Neutral KCl Electrolytes. *J. Am. Chem. Soc.* **2021**, *143* (8), 3245−3255.
(3) Niu, Z.-Z.; Gao, F.; Zhang, X.; Yang, P.; Liu, R.; Chi, L.; Wu, Z.; Qin, S.; Yu, X.; Gao, M. Hierarchical Copper with Inherent Hydrophobicity Mitigates Electrode Flooding for High-Rate CO_2 Electroreduction to Multicarbon Products. *J. Am. Chem. Soc.* **2021**, *143* (21), 8011−8021.
(4) Gao, D.; Arán-Ais, R. M.; Jeon, H. S.; Cuenya, B. R. Rational catalyst and electrolyte design for CO_2 electroreduction towards multicarbon products. *Nat. Catal.* **2019**, *2* (3), 198−210.
(5) Bondue, C. J.; Graf, M.; Goyal, A.; Koper, M. T. M. Suppression of Hydrogen Evolution in Acidic Electrolytes by Electrochemical CO_2 Reduction. *J. Am. Chem. Soc.* **2021**, *143* (1), 279−285.
(6) Xie, Y.; Ou, P.; Wang, X.; Xu, Z.; Li, Y. C.; Wang, Z.; Huang, J. E.; Wicks, J.; McCallum, C.; Wang, N.; Wang, Y.; Chen, T.; Lo, B. T. W.; Sinton, D.; Yu, J. C.; Wang, Y.; Sargent, E. H. High Carbon Utilization in CO_2 Reduction to Multi-Carbon Products in Acidic Media. *Nat. Catal.* **2022**, *5* (6), 564−570.
(7) Gao, S.; Chen, S.; Liu, Q.; Zhang, S.; Qi, G.; Luo, J.; Liu, X. Bifunctional BiPd Alloy Particles Anchored on Carbon Matrix for Reversible Zn−CO_2 Battery. *ACS Appl. Nano Mater.* **2022**, *5* (9), 12387−12394.
(8) Gao, S.; Wang, T.; Jin, M.; Zhang, S.; Liu, Q.; Hu, G.; Yang, H.; Luo, J.; Liu, X. Bifunctional Nb-N-C atomic catalyst for aqueous Zn-air battery driving CO_2 electrolysis. *Sci. China Mater.* **2023**, *66* (3), 1013−1023.
(9) Gotico, P.; Roupnel, L.; Guillot, R.; Sircoglou, M.; Leibl, W.; Halime, Z.; Aukauloo, A. Atropisomeric Hydrogen Bonding Control for CO_2 Binding and Enhancement of Electrocatalytic Reduction at Iron Porphyrins. *Angew. Chem., Int. Ed.* **2020**, *59* (50), 22451−22455.
(10) He, C.; Zhang, Y.; Zhang, Y.; Zhao, L.; Yuan, L.-P.; Zhang, J.; Ma, J.; Hu, J. Molecular Evidence for Metallic Cobalt Boosting CO_2 Electroreduction on Pyridinic Nitrogen. *Angew. Chem., Int. Ed.* **2020**, *59* (12), 4914−4919.
(11) Yang, M.; Sun, J.; Qin, Y.; Yang, H.; Zhang, S.; Liu, X.; Luo, J. Hollow CoFe-layered double hydroxide polyhedrons for highly efficient CO_2 electrolysis. *Sci. China Mater.* **2022**, *65* (2), 536−542.
(12) Kang, X.; Li, L.; Sheveleva, A.; Han, X.; Li, J.; Liu, L.; Tuna, F.; McInnes, E. J. L.; Han, B.; Yang, S.; Schröder, M. Electro-Reduction of Carbon Dioxide at Low Over-Potential at a Metal-Organic Framework Decorated Cathode. *Nat. Commun.* **2020**, *11* (1), No. 5464.
(13) Shang, H.; Wang, T.; Pei, J.; Jiang, Z.; Zhou, D.; Wang, Y.; Li, H.; Dong, J.; Zhuang, Z.; Chen, W.; Wang, D.; Zhang, J.; Li, Y. Design of a Single-Atom Indium$^{\delta+}$−N_4 Interface for Efficient Electroreduction of CO_2 to Formate. *Angew. Chem., Int. Ed.* **2020**, *59* (50), 22465−22469.
(14) Wang, X.; Liu, S.; Zhang, H.; Zhang, S.; Meng, G.; Liu, Q.; Sun, Z.; Luo, J.; Liu, X. Polycrystalline SnSx nanofilm enables CO_2 electroreduction to formate with high current density. *Chem. Commun.* **2022**, *58* (55), 7654−7657.
(15) Chen, S.; Li, W.; Jiang, W.; Yang, J.; Zhu, J.; Wang, L.; Ou, H.; Zhuang, Z.; Chen, M.; Sun, X.; Wang, D.; Li, Y. MOF Encapsulating N-Heterocyclic Carbene-Ligated Copper Single-Atom Site Catalyst towards Efficient Methane Electrosynthesis. *Angew. Chem., Int. Ed.* **2022**, *61* (4), No. e202114450, DOI: 10.1002/anie.202114450.
(16) Liu, S.; Zhang, B.; Zhang, L.; Sun, J. Rational design strategies of Cu-based electrocatalysts for CO_2 electroreduction to C_2 products. *J. Energy Chem.* **2022**, *71*, 63−82.
(17) Peng, C.; Luo, G.; Xu, Z.; Yan, S.; Zhang, J.; Chen, M.; Qian, L.; Wei, W.; Han, Q.; Zheng, G. Lithiation-Enabled High-Density Nitrogen Vacancies Electrocatalyze CO_2 to C_2 Products. *Adv. Mater.* **2021**, *33* (40), No. 2103150.
(18) Popović, S.; Smiljanić, M.; Jovanovič, P.; Vavra, J.; Buonsanti, R.; Hodnik, N. Stability and Degradation Mechanisms of Copper-Based Catalysts for Electrochemical CO_2 Reduction. *Angew. Chem., Int. Ed.* **2020**, *59* (35), 14736−14746.
(19) Wang, C.; Lv, Z.; Yang, W.; Feng, X.; Wang, B. A Rational Design of Functional Porous Frameworks for Electrocatalytic CO_2 Reduction Reaction. *Chem. Soc. Rev.* **2023**, *52* (4), 1382−1427.
(20) Quan, W.; Lin, Y.; Luo, Y.; Huang, Y. Electrochemical CO_2 Reduction on Cu: Synthesis-Controlled Structure Preference and Selectivity. *Adv. Sci.* **2021**, *8* (23), No. 2101597.
(21) Huang, D.-S.; Zhu, H.; Zhao, Z.; Huang, J.; Liao, P.; Chen, X. A Stable and Low-Cost Metal-Azolate Framework with Cyclic Tricopper Active Sites for Highly Selective CO_2 Electroreduction to C_{2+} Products. *ACS Catal.* **2022**, *12* (14), 8444−8450.
(22) Woldu, A. R.; Huang, Z.; Zhao, P.; Hu, L.; Astruc, D. Electrochemical CO_2 reduction (CO_2RR) to multi-carbon products over copper-based catalysts. *Coord. Chem. Rev.* **2022**, *454*, No. 214340.
(23) Zhang, Y.; Dong, L.; Li, S.; Huang, X.; Chang, J.; Wang, J.; Zhou, J.; Li, S.; Lan, Y. Coordination Environment Dependent Selectivity of Single-Site-Cu Enriched Crystalline Porous Catalysts in CO_2 Reduction to CH_4. *Nat. Commun.* **2021**, *12* (1), No. 6390.
(24) Sun, S.-N.; Lu, J.-N.; Li, Q.; Dong, L.; Huang, Q.; Liu, J.; Lan, Y. Establishing Spatially Elastic Hydrogen-Bonding Interaction in

Electrochemical Process for Selective CO_2-To-CH_4 Conversion. *Chem. Catal.* **2021**, *1* (5), 1133−1144.
(25) Wang, R.; Liu, J.; Huang, Q.; Dong, L.; Li, S.; Lan, Y. Partial Coordination-Perturbed Bi-Copper Sites for Selective Electroreduction of CO_2 to Hydrocarbons. *Angew. Chem., Int. Ed.* **2021**, *60* (36), 19829−19835.
(26) Lu, Y.; Dong, L.; Liu, J.; Yang, R.; Liu, J.; Zhang, Y.; Zhang, L.; Wang, Y.; Li, S.; Lan, Y. Predesign of Catalytically Active Sites via Stable Coordination Cluster Model System for Electroreduction of CO_2 to Ethylene. *Angew. Chem., Int. Ed.* **2021**, *60* (50), 26210−26217.
(27) Wang, R.; Liu, J.; Dong, L.; Zhou, J.; Huang, Q.; Wang, Y.; Shi, J.; Lan, Y. Selective Generation of Electroreduction C_1−C_2 Products Through Self-Regulation of Catalytically Active Cu Sites on the Same Coordination Cluster Catalyst. *CCS Chem.* **2023**, *5*, 2237−2250, DOI: 10.31635/ccschem.022.202202316.
(28) Peng, H.-J.; Tang, M. T.; Halldin Stenlid, J.; Liu, X.; Abild-Pedersen, F. Trends in oxygenate/hydrocarbon selectivity for electrochemical $CO_{(2)}$ reduction to C_2 products. *Nat. Commun.* **2022**, *13* (1), No. 1399.
(29) Wang, Y.; Wang, Q.; Wu, J.; Zhao, X.; Xiong, Y.; Luo, F.; Lei, Y. Asymmetric Atomic Sites Make Different: Recent Progress in Electrocatalytic CO_2 Reduction. *Nano Energy* **2022**, *103*, No. 107815.
(30) Wang, Y.; Liu, M.; Gao, G.; Yang, Y.; Yang, R.; Ding, H.; Chen, Y.; Li, S.; Lan, Y. Implanting Numerous Hydrogen-Bonding Networks in a Cu-Porphyrin-Based Nanosheet to Boost CH_4 Selectivity in Neutral-Media CO_2 Electroreduction. *Angew. Chem., Int. Ed.* **2021**, *60* (40), 21952−21958.
(31) Dong, L.-Z.; Lu, Y.; Wang, R.; Zhou, J.; Zhang, Y.; Zhang, L.; Liu, J.; Li, S.; Lan, Y. Porous Copper Cluster-Based MOF with Strong Cuprophilic Interactions for Highly Selective Electrocatalytic Reduction of CO_2 to CH_4. *Nano Res.* **2022**, *15* (12), 10185−10193.
(32) Zhang, X.-D.; Liu, T.; Liu, C.; Zheng, D.; Huang, J.; Liu, Q.; Yuan, W.; Yin, Y.; Huang, L.; Xu, M.; Li, Y.; Gu, Z. Asymmetric Low-Frequency Pulsed Strategy Enables Ultralong CO_2 Reduction Stability and Controllable Product Selectivity. *J. Am. Chem. Soc.* **2023**, *145* (4), 2195−2206.
(33) Li, F.; Li, Y. C.; Wang, Z.; Li, J.; Nam, D.; Lum, Y.; Luo, M.; Wang, X.; Ozden, A.; Hung, S.; Chen, B.; Wang, Y.; Wicks, J.; Xu, Y.; Li, Y.; Gabardo, C. M.; Dinh, C.; Wang, Y.; Zhuang, T.; Sinton, D.; Sargent, E. H. Cooperative CO_2-to-Ethanol Conversion via Enriched Intermediates at Molecule−Metal Catalyst Interfaces. *Nat. Catal.* **2020**, *3* (1), 75−82.
(34) Ma, G.; Syzgantseva, O. A.; Huang, Y.; Stoian, D.; Zhang, J.; Yang, S.; Luo, W.; Jiang, M.; Li, S.; Chen, C.; Syzgantseva, M. A.; Yan, S.; Chen, N.; Peng, L.; Li, J.; Han, B. A hydrophobic Cu/Cu_2O sheet catalyst for selective electroreduction of CO to ethanol. *Nat. Commun.* **2023**, *14* (1), No. 501.
(35) Zhang, X.; Zhang, Z.; Li, H.; Gao, R.; Xiao, M.; Zhu, J.; Feng, M.; Chen, Z. Insight Into Heterogeneous Electrocatalyst Design Understanding for the Reduction of Carbon Dioxide. *Adv. Energy Mater.* **2022**, *12* (39), No. 2201461.
(36) Zhou, Y.; Che, F.; Liu, M.; Zou, C.; Liang, Z.; De Luna, P.; Yuan, H.; Li, J.; Wang, Z.; Xie, H.; Li, H.; Chen, P.; Bladt, E.; Quintero-Bermudez, R.; Sham, T.-K.; Bals, S.; Hofkens, J.; Sinton, D.; Chen, G.; Sargent, E. H. Dopant-induced electron localization drives CO_2 reduction to C_2 hydrocarbons. *Nat. Chem.* **2018**, *10* (9), 974−980.
(37) Dinh, C.-T.; Burdyny, T.; Kibria, M. G.; Seifitokaldani, A.; Gabardo, C. M.; García de Arquer, F. P.; Kiani, A.; Edwards, J. P.; De Luna, P.; Bushuyev, O. S.; Zou, C.; Quintero-Bermudez, R.; Pang, Y.; Sinton, D.; Sargent, E. H. CO_2 Electroreduction to Ethylene via Hydroxide-Mediated Copper Catalysis at an Abrupt Interface. *Science* **2018**, *360* (6390), 783−787.
(38) Lv, J.; Yin, R.; Zhou, L.; Li, J.; Kikas, R.; Xu, T.; Wang, Z.; Jin, H.; Wang, X.; Wang, S. Microenvironment Engineering for the Electrocatalytic CO_2 Reduction Reaction. *Angew. Chem., Int. Ed.* **2022**, *61* (39), No. e202207252.
(39) Liu, Z.; Yan, T.; Shi, H.; Pan, H.; Cheng, Y.; Kang, P. Acidic Electrocatalytic CO_2 Reduction Using Space-Confined Nanoreactors. *ACS Appl. Mater. Interfaces* **2022**, *14* (6), 7900−7908.
(40) Huang, J. E.; Li, F.; Ozden, A.; Sedighian Rasouli, A.; García de Arquer, F. P.; Liu, S.; Zhang, S.; Luo, M.; Wang, X.; Lum, Y.; Xu, Y.; Bertens, K.; Miao, R. K.; Dinh, C.-T.; Sinton, D.; Sargent, E. H. CO_2 electrolysis to multicarbon products in strong acid. *Science* **2021**, *372* (6546), 1074−1078.
(41) Wang, P.; Yang, H.; Tang, C.; Wu, Y.; Zheng, Y.; Cheng, T.; Davey, K.; Huang, X.; Qiao, S. Boosting Electrocatalytic CO_2−to−Ethanol Production via Asymmetric C−C Coupling. *Nat. Commun.* **2022**, *13* (1), No. 3754.
(42) Li, Z.; Yang, Y.; Yin, Z.; Wei, X.; Peng, H.; Lyu, K.; Wei, F.; Xiao, L.; Wang, G.; Abruña, H. D.; Lu, J.; Zhuang, L. Interface-Enhanced Catalytic Selectivity on the C_2 Products of CO_2 Electroreduction. *ACS Catal.* **2021**, *11* (5), 2473−2482.
(43) Yi, J.; Xie, R.; Xie, Z.; Chai, G.; Liu, T.; Chen, R.; Huang, Y.; Cao, R. Highly Selective CO_2 Electroreduction to CH_4 by *In Situ* Generated Cu_2O Single-Type Sites on a Conductive MOF: Stabilizing Key Intermediates with Hydrogen Bonding. *Angew. Chem., Int. Ed.* **2020**, *59* (52), 23641−23648.
(44) Yang, B.; Chen, L.; Xue, S.; Sun, H.; Feng, K.; Chen, Y.; Zhang, X.; Xiao, L.; Qin, Y.; Zhong, J.; Deng, Z.; Jiao, Y.; Peng, Y. Electrocatalytic CO_2 Reduction to Alcohols by Modulating the Molecular Geometry and Cu Coordination in Bicentric Copper Complexes. *Nat. Commun.* **2022**, *13* (1), No. 5122.
(45) Pérez-Gallent, E.; Figueiredo, M. C.; Calle-Vallejo, F.; Koper, M. T. M. Spectroscopic Observation of a Hydrogenated CO Dimer Intermediate During CO Reduction on Cu(100) Electrodes. *Angew. Chem., Int. Ed.* **2017**, *56* (13), 3621−3624.
(46) Liu, Y.; Chen, S.; Quan, X.; Yu, H. Efficient Electrochemical Reduction of Carbon Dioxide to Acetate on Nitrogen-Doped Nanodiamond. *J. Am. Chem. Soc.* **2015**, *137* (36), 11631−11636.
(47) Su, X.; Jiang, Z.; Zhou, J.; Liu, H.; Zhou, D.; Shang, H.; Ni, X.; Peng, Z.; Yang, F.; Chen, W.; Qi, Z.; Wang, D.; Wang, Y. Complementary Operando Spectroscopy Identification of In-Situ Generated Metastable Charge-Asymmetry Cu_2-CuN_3 Clusters for CO_2 Reduction to Ethanol. *Nat. Commun.* **2022**, *13* (1), No. 1322.
(48) Huang, D. S.; Zhu, H. L.; Zhao, Z. H.; Huang, J. R.; Liao, P. Q.; Chen, X. M. A Stable and Low-Cost Metal-Azolate Framework with Cyclic Tricopper Active Sites for Highly Selective CO_2 Electroreduction to C_{2+} Products. *ACS Catal.* **2022**, *12* (14), 8444−8450.
(49) Kim, J. Y.; Kim, G.; Won, H.; Gereige, I.; Jung, W.-B.; Jung, H.-T. Synergistic Effect of Cu_2O Mesh Pattern on High-Facet Cu Surface for Selective CO_2 Electroreduction to Ethanol. *Adv. Mater.* **2022**, *34* (3), No. 2106028.
(50) Wang, P.; Yang, H.; Tang, C.; Wu, Y.; Zheng, Y.; Cheng, T.; Davey, K.; Huang, X.; Qiao, S.-Z. Boosting electrocatalytic CO_2−to−ethanol production via asymmetric C−C coupling. *Nat. Commun.* **2022**, *13* (1), No. 3754.
(51) Yin, J.; Yin, Z.; Jin, J.; Sun, M.; Huang, B.; Lin, H.; Ma, Z.; Muzzio, M.; Shen, M.; Yu, C.; Zhang, H.; Peng, Y.; Xi, P.; Yan, C.-H.; Sun, S. A New Hexagonal Cobalt Nanosheet Catalyst for Selective CO_2 Conversion to Ethanal. *J. Am. Chem. Soc.* **2021**, *143* (37), 15335−15343.

https://doi.org/10.1021/acscatal.3c03755
ACS Catal. 2024, 14, 741−750